CFD-Based Performance Assessment of Flanged Diffuser Configurations for a Horizontal-Axis Marine Current Turbine

Najdan Waris Chappayil* and Jaswanth T. M

India

* Correspondence: najdanwariscp@gmail.com

Abstract

Marine current turbines can provide predictable renewable power, but their performance at moderate current speeds depends strongly on the flow delivered to the rotor. This study numerically evaluates an open horizontal-axis marine current turbine and two flanged diffuser configurations with short and long expansion sections. Three-dimensional geometries were created in SOLIDWORKS and analysed in ANSYS CFX using a steady-state Reynolds-averaged Navier-Stokes approach with the shear-stress-transport turbulence model. The turbine employed a NACA 63-4XX blade profile, a rotor radius of 2.2 m, a hub ratio of 0.2, and a design tip-speed ratio of 5.1. The inlet current speed was specified as 3 m/s. The reported pressure drop increased from 1475.5 Pa for the open turbine to 5599 Pa for the short diffuser and 9802 Pa for the long diffuser. Flow contours indicate that the flange generates a downstream low-pressure region and vortex structures that draw flow towards the rotor. Within the limits of the steady numerical model, the long-expansion configuration produced the largest pressure difference and therefore the strongest indication of available pressure-energy conversion. Further work should quantify torque and power coefficient, establish mesh independence, validate the model experimentally, and assess cavitation and bidirectional tidal operation.
Keywords: marine current turbine; tidal-stream energy; flanged diffuser; ducted turbine; computational fluid dynamics; ANSYS CFX; flow augmentation

1. Introduction

The transition from fossil-fuel-based electricity generation has intensified interest in predictable renewable resources. Marine currents are attractive because their kinetic energy can be converted by submerged turbines using principles similar to wind-energy conversion, while the greater density of water permits substantial rotor loading at comparatively low flow speeds (Bahaj and Myers, 2003; Batten et al., 2006). Unlike barrage systems, tidal-stream devices extract kinetic energy directly from moving water and can be deployed without impounding an estuary.

Horizontal-axis marine current turbines are widely studied because they can achieve relatively high hydrodynamic efficiency and low torque fluctuation. Nevertheless, practical designs must address cyclic loading, cavitation, harsh marine exposure, wake interaction, installation constraints, and the need for acceptable performance over a range of current speeds (Batten et al., 2006; Satrio et al., 2016; Nicholls-Lee et al., 2006). One approach to improving rotor inflow is to surround the turbine with a diffuser or shroud. A divergent duct can create a lower-pressure region downstream of the rotor, while a flange at the diffuser exit can strengthen vortex formation and increase mass flow through the rotor plane (Ohya et al., 2008; Abe et al., 2005; Matsushima et al., 2006; El-Zahaby et al., 2017; Al-Quraishi et al., 2018).

Most early diffuser-development studies were conducted for wind turbines, but the underlying flow-augmentation concept is relevant to hydrokinetic devices. The present work compares an unshrouded turbine with short- and long-expansion flanged diffuser configurations. The objective is to determine how diffuser length influences the pressure and velocity fields around a horizontal-axis marine current turbine under a common numerical setup. The principal contribution is a direct three-configuration comparison based on the same rotor geometry and inlet condition.

1.1. Recent developments and research gap

Recent research shows that marine-current technology is progressing from prototype development toward larger devices and array-level deployment, while blade optimization, drivetrain selection, test infrastructure, reliability and commercial viability remain important challenges (Gu et al., 2024). Full-scale testing and modelling have also demonstrated the importance of representing power, torque and thrust characteristics under realistic operating conditions (Diaz-Dorado et al., 2021). Site-specific resource assessment and hydrodynamic blade design remain closely connected because the rotor geometry must be matched to the available current regime (Hazim et al., 2021).

For ducted and diffuser-augmented turbines, performance depends on diffuser efficiency, separation behaviour, base pressure and interactions between the rotor and surrounding structure (Shives and Crawford, 2012). Experimental work has confirmed that diffuser angle affects the power coefficient and that numerical predictions require physical validation (Ambarita et al., 2022). Recent numerical investigations have further highlighted wake structure, turbulent intensity, vorticity identification and entropy production in diffuser-augmented tidal turbines (Zang et al., 2023). Multi-objective studies also indicate that diffuser geometry should be evaluated against both efficiency and cavitation considerations (Ambarita et al., 2021).

1.2. Contribution of the present study

Against this background, the present study provides a controlled three-configuration comparison using one open rotor and two flanged diffusers with different expansion lengths. The contribution is focused on the corresponding pressure and velocity fields under a common numerical setup. The study does not treat pressure difference as a direct substitute for turbine efficiency; instead, it identifies the flow-augmentation mechanism and establishes the additional torque, power-coefficient, mesh-independence, cavitation and validation work required for a defensible performance claim.

2. . Materials and Methods

2.1. Turbine and Diffuser Geometry

The rotor and diffuser geometries were created in SOLIDWORKS. The baseline model comprised a horizontal-axis rotor with a streamlined hub. Two augmented configurations were then constructed by adding axisymmetric divergent shrouds with a flange at the diffuser exit. The short and long configurations had the same divergent angle, blade-tip clearance, and flange height, but different diffuser lengths.

Fig. 1. Baseline open-turbine CAD configuration.

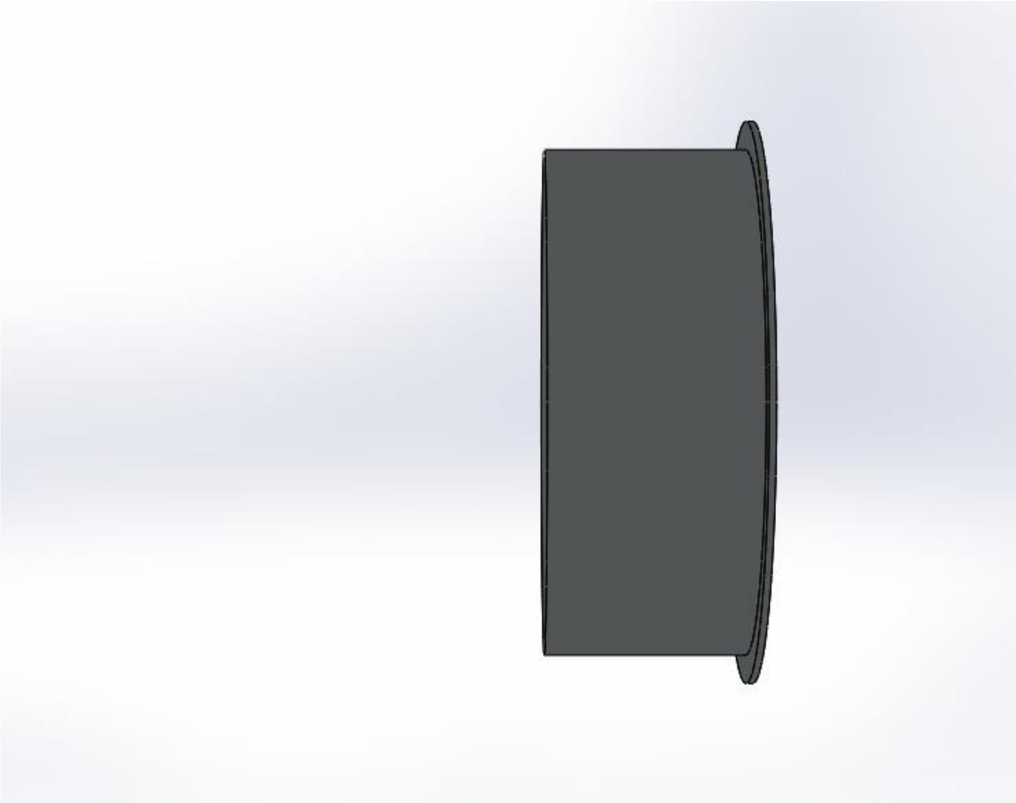

Fig. 2. Short-expansion flanged-diffuser configuration.

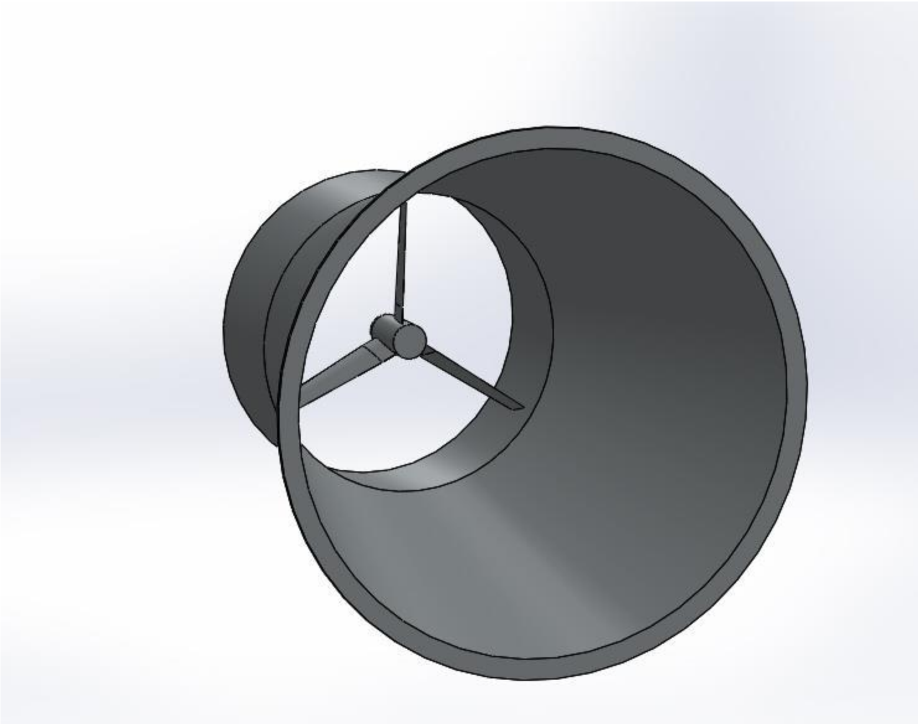

Fig. 3. Long-expansion flanged-diffuser configuration.

Table 1. Principal turbine and diffuser parameters reported in the project study.

Parameter	Value
Blade profile	NACA 63-4XX
Rotor radius, r	2.2 m
Hub ratio	0.2
Design tip-speed ratio	5.1
Diffuser divergent angle	15 degrees
Blade-tip clearance	0.02 m
Short diffuser length	0.078 m
Long diffuser length	0.318 m
Flange height	0.013 m

2.2. Blade Angle Selection

A two-dimensional hydrofoil assessment was used to compare lift-to-drag ratio over a range of angles of attack. The highest reported lift-to-drag ratio was 29.63 at 6 degrees; accordingly, 6 degrees was selected as the design angle for the model. The underlying coefficient values should be rechecked against the original solver exports before journal submission because the reported lift and drag coefficient magnitudes are unusually large for dimensionless aerodynamic coefficients.

Table 2. Reported lift-to-drag ratio used for angle selection.

Angle of attack (degrees)	Reported CL/CD
0	-0.053
2	17.289
4	11.656
5	29.076
6	29.631
8	28.289
10	26.863
15	17.795
16	6.698

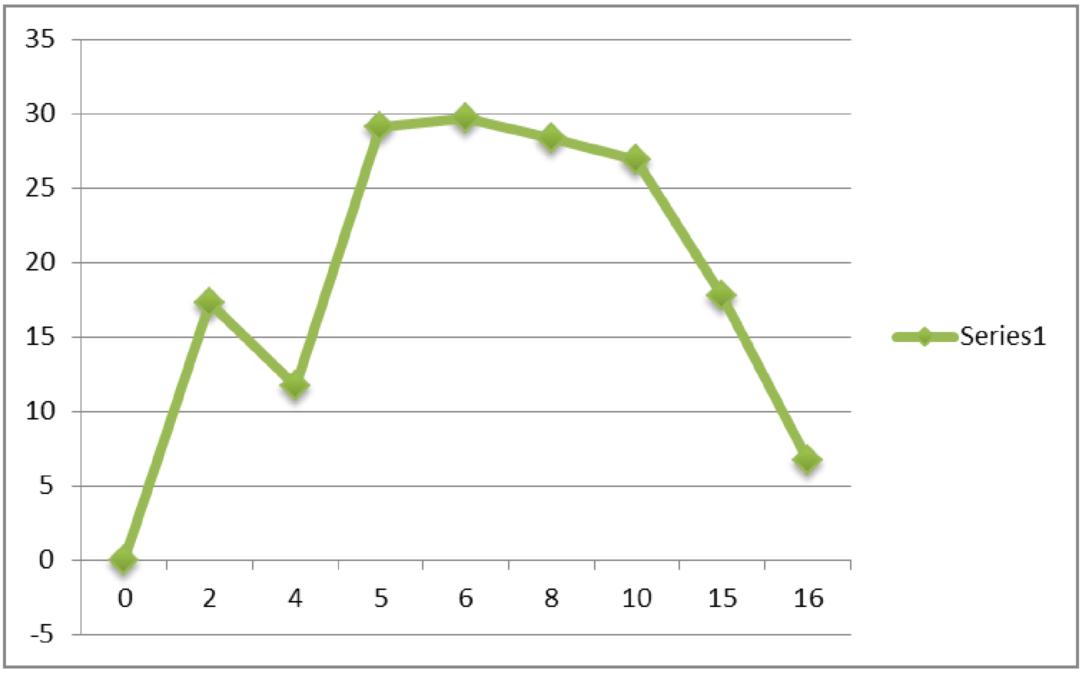

Fig. 4. Reported variation of lift-to-drag ratio with angle of attack.

2.3. Computational Domain and Mesh

The turbine was placed inside a cylindrical stationary fluid domain. The report specifies a domain diameter of 1500 mm and length of 900 mm, with tetrahedral elements, a global mesh size of 10 mm, and local face sizing of 2 mm. These dimensions appear inconsistent with the reported rotor radius of 2.2 m and must be verified against the original CAD and ANSYS files before submission. The domain was intended to be sufficiently large to reduce wall effects.

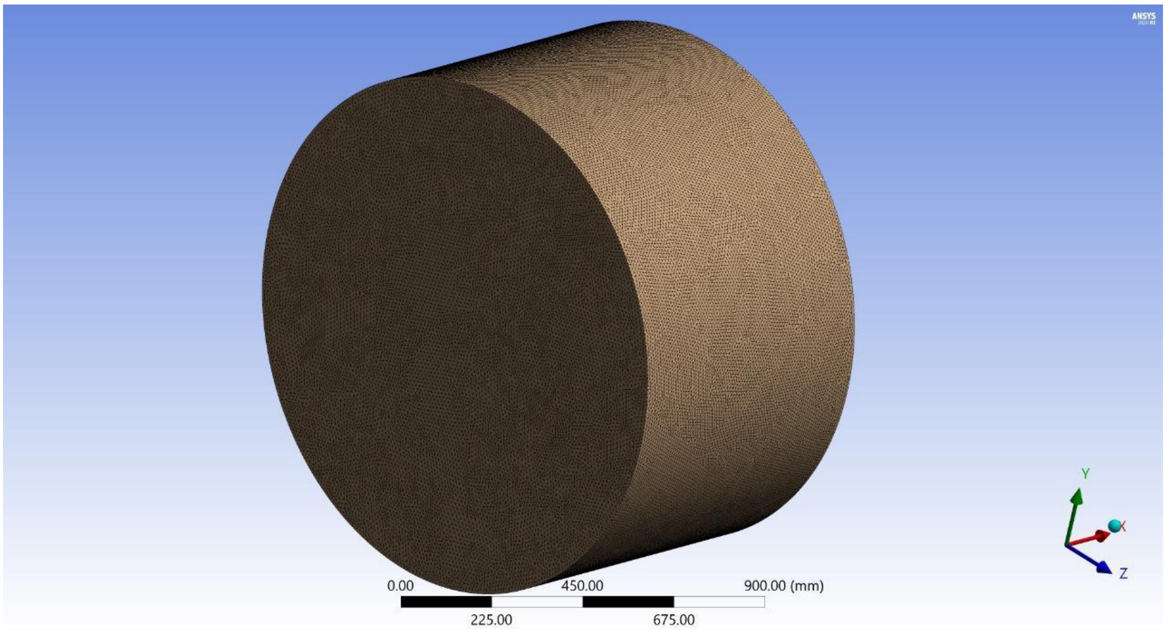

Fig. 5. Generated mesh of the computational domain.

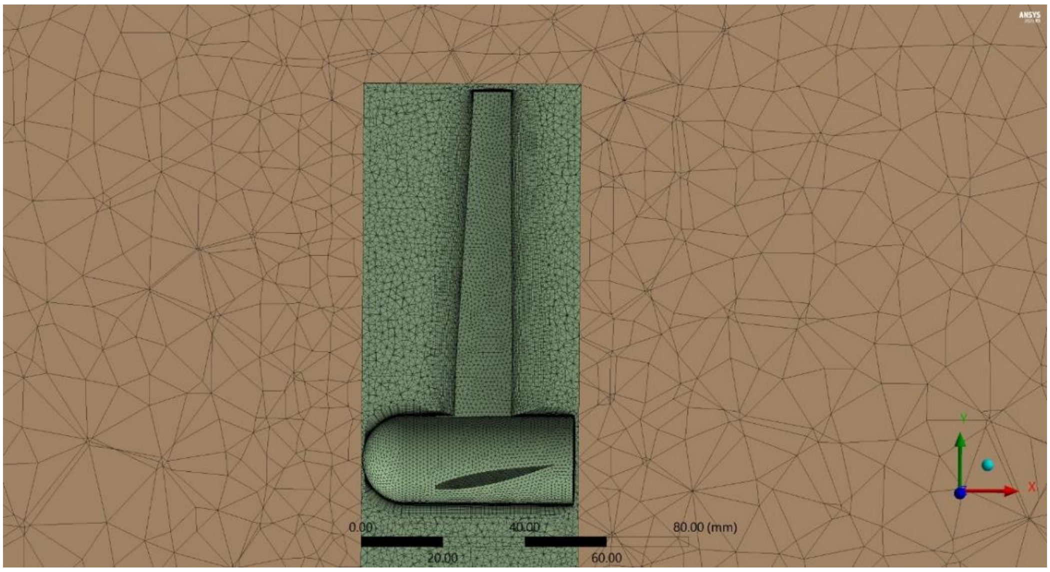

Fig. 6. Generated mesh around the turbine.

2.4. Governing Approach and Boundary Conditions

The flow was solved in ANSYS CFX using a pressure-based, steady-state formulation. The shear-stress-transport turbulence model was selected. Water entered the domain at a specified speed of 3 m/s. Solid walls were treated as smooth no-slip surfaces, and the turbine was reported at a depth of 3 m. The original report does not provide fluid properties, rotor rotational speed, rotating-domain treatment, interface settings, convergence criteria, residual histories, time-scale control, or outlet boundary specification. These items are required for full reproducibility and should be recovered from the ANSYS case files.

3. 3. Results

3.1. Pressure Field

For the open turbine, the reported pressure decreased from 1068 Pa upstream to -407.5 Pa downstream, corresponding to a pressure difference of 1475.5 Pa. The contour shows the expected pressure contrast across the blade region and a downstream wake.

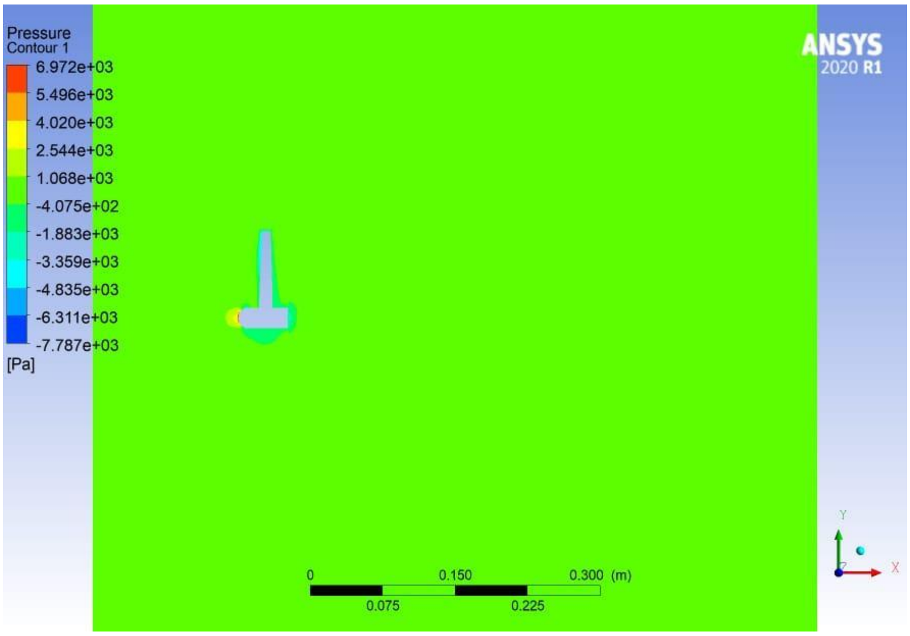

Fig. 7. Pressure contour for the open-turbine configuration.

For the short-expansion diffuser, the reported upstream and downstream pressures were 1010 Pa and -4589 Pa, respectively, giving a pressure difference of 5599 Pa. The low-pressure region downstream of the flange was associated with vortex formation and flow attraction towards the rotor axis.

Fig. 8. Pressure contour for the short-expansion flanged diffuser.

For the long-expansion diffuser, the corresponding pressures were 2267 Pa and -7535 Pa, yielding the largest reported pressure difference of 9802 Pa. The longer expansion section produced a broader pressure-recovery region downstream of the rotor while maintaining a low-pressure zone near the flange.

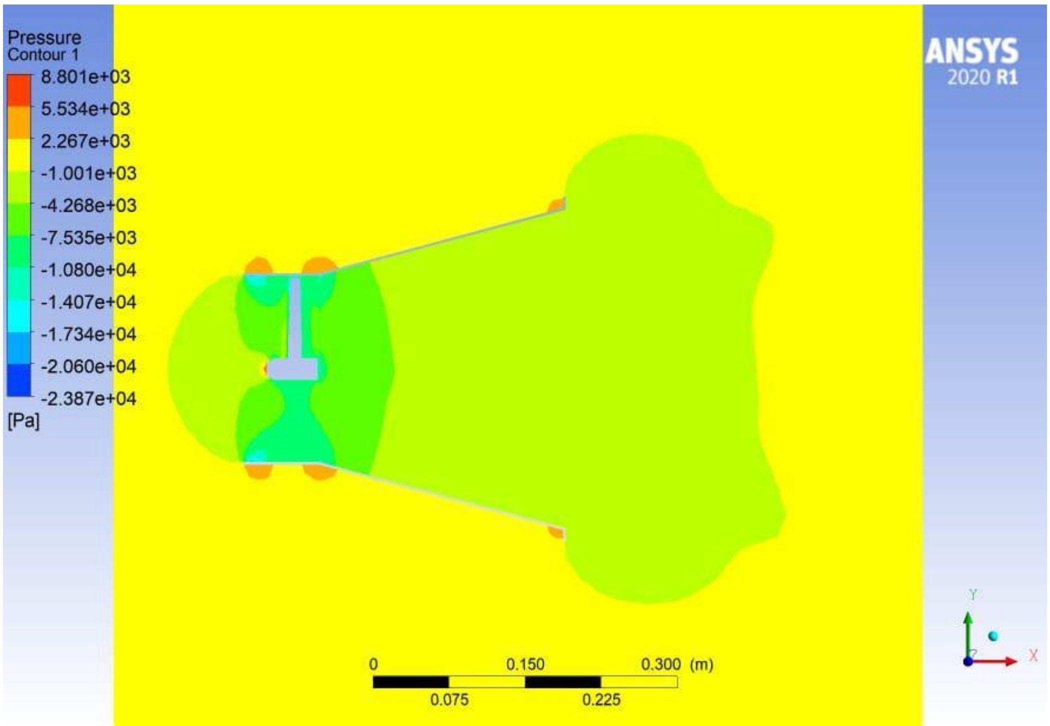

Fig. 9. Pressure contour for the long-expansion flanged diffuser.

Table 3. Summary of reported pressure values.

Configuration	Upstream pressure (Pa)	Downstream pressure (Pa)	Reported difference (Pa)
Open turbine	1068	-407.5	1475.5
Short expansion	1010	-4589	5599
Long expansion	2267	-7535	9802

3.2. Velocity Field

The open-turbine contour reported an inlet-side velocity of 3.02 m/s and a local velocity of 3.45 m/s around the turbine, an increase of 0.43 m/s. The wake behind the hub showed reduced velocity.

Fig. 10. Velocity field for the open-turbine configuration.

For the short diffuser, the reported velocity increased from 3.55 m/s at the inlet side to 4.70 m/s around the turbine. This local acceleration is consistent with the pressure depression generated by the flanged diffuser.

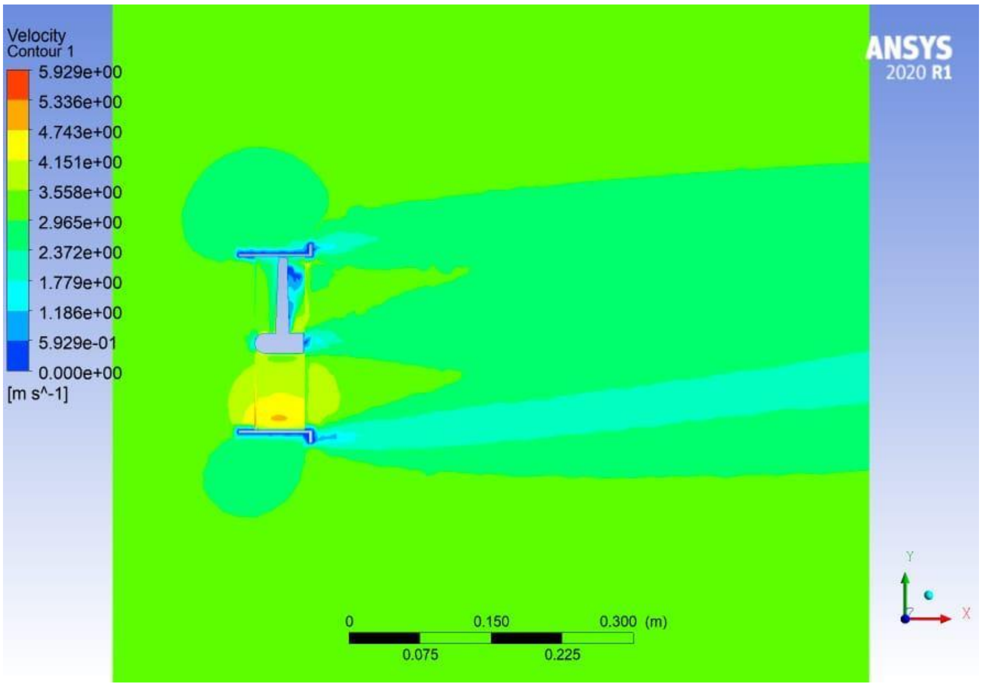

Fig. 11. Velocity field for the short-expansion flanged diffuser.

The long-diffuser section in the source report lists 3.864 m/s and 2.325 m/s and labels their difference as a 1.535 m/s increase. Numerically, the second value is lower than the first, so the direction and sampling locations must be verified against the CFX results. The contour nevertheless indicates non-uniform acceleration near the rotor and deceleration during downstream pressure recovery.

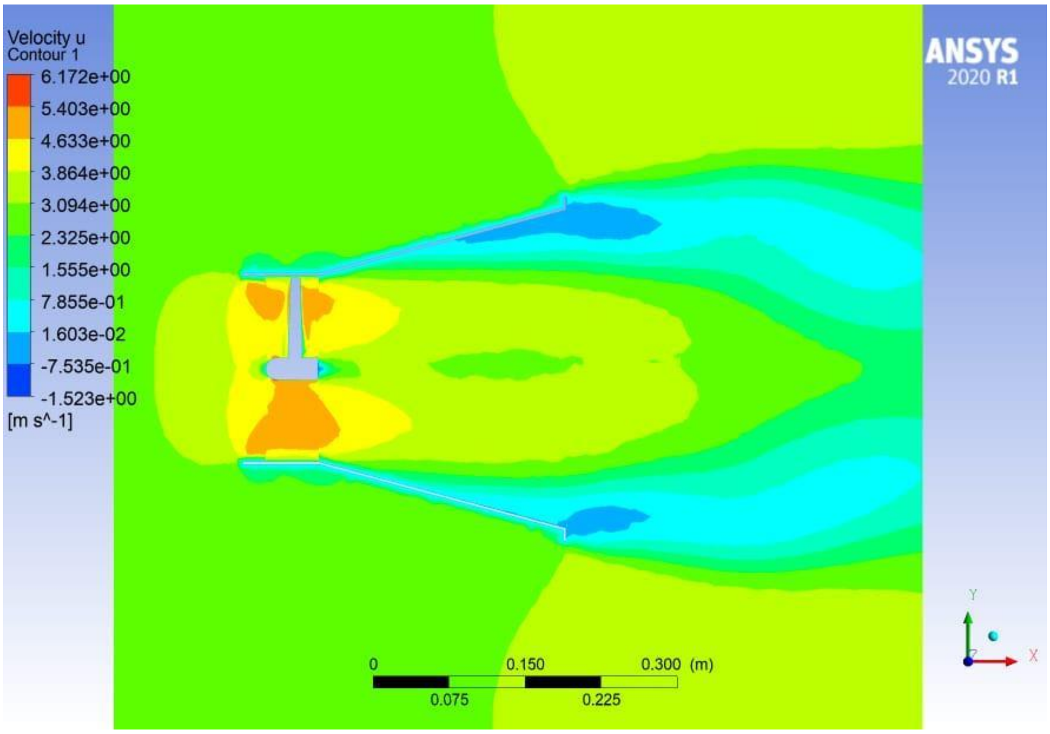

Fig. 12. Velocity field for the long-expansion flanged diffuser.

Table 4. Reported velocity values and editorial interpretation.

Configuration	Reported inlet-side velocity (m/s)	Reported local velocity (m/s)	Interpretation
Open turbine	3.02	3.45	Local increase of 0.43 m/s
Short expansion	3.55	4.70	Local increase of 1.15 m/s
Long expansion	3.864	2.325	Values require verification

4. Discussion

The numerical comparison indicates that adding a flanged diffuser substantially changes the pressure field around the rotor. Relative to the open configuration, the reported pressure difference was approximately 3.8 times greater for the short diffuser and 6.6 times greater for the long diffuser. These ratios quantify pressure-field change only; they should not be interpreted directly as power-coefficient or efficiency gains without rotor torque, angular speed, mass-flow rate, and a consistent reference area.

The observed mechanism is consistent with diffuser-augmented turbine concepts reported in the literature. Flow separation and vortex formation behind the flange create a low-pressure region that draws additional fluid through the diffuser (Ohya et al., 2008; Abe et al., 2005; Matsushima et al., 2006; El-Zahaby et al., 2017; Al-Quraishi et al., 2018). Increasing diffuser length can also improve pressure recovery downstream. However, excessive expansion can cause separation, increased structural loads, and increased cost. Therefore, the longest geometry tested should be described as the best-performing configuration within the present comparison, not necessarily as the globally optimal design.

Several limitations must be addressed before the study is ready for peer review. First, the computational-domain dimensions and rotor dimensions must be reconciled. Second, a mesh-independence study is needed, together with near-wall resolution and y-plus reporting. Third, model convergence, rotating-frame treatment, and numerical uncertainty must be documented. Fourth, the simulations should be validated against experimental data or a published benchmark. Fifth, performance should be reported using torque coefficient, thrust coefficient, and power coefficient across several tip-speed ratios. Finally, cavitation risk, diffuser structural loading, blockage, free-surface effects, and bidirectional tidal flow require assessment.

The interpretation is consistent with recent diffuser-augmented turbine studies. Zang et al. (2023) reported that the diffuser and supporting structures influence wake development, turbulent intensity and entropy production, whereas Ambarita et al. (2022) experimentally demonstrated that diffuser-angle selection changes the achievable power coefficient. Tahani et al. (2023) likewise examined a diffuser-augmented horizontal-axis tidal turbine using ANSYS CFX and the SST turbulence model. These studies reinforce the need to connect the present pressure and velocity observations to verified torque, thrust and power coefficients rather than relying on pressure difference alone.

The wider literature also shows that credible marine-current turbine assessment should combine hydrodynamic design, realistic operating conditions and numerical verification. Recent full-scale and site-specific studies have addressed counter-rotating turbine modelling, resource-oriented rotor design, mesh independence and performance prediction (Diaz-Dorado et al., 2021; Hazim et al., 2021; Munna and Uddin, 2025). The current results therefore provide a preliminary comparative basis, while the next stage should include a verified computational domain, documented convergence, mesh sensitivity, near-wall resolution, torque and thrust extraction, power-coefficient curves over several tip-speed ratios, and experimental or benchmark validation.

5. Conclusions

A CFD comparison of an open marine current turbine and two flanged diffuser configurations was completed using ANSYS CFX. Under the reported common inlet condition, the pressure difference increased from 1475.5 Pa for the open turbine to 5599 Pa for the short diffuser and 9802 Pa for the long diffuser. The contours associate this increase with a downstream low-pressure region and vortex formation near the diffuser flange. Among the three configurations tested, the long-expansion model produced the largest reported pressure difference. The present findings support further investigation of flanged diffusers for marine-current applications, but a journal-level claim of improved efficiency requires verified geometry, numerical convergence, mesh independence, torque and power calculations, and experimental or benchmark validation.

References

1. Bahaj, A.S.; Myers, L.E. Fundamentals applicable to the utilisation of marine current turbines for energy production. Renewable Energy 2003, 28, 2205-2211.
2. Batten, W.M.J.; Bahaj, A.S.; Molland, A.F.; Chaplin, J.R. Hydrodynamics of marine current turbines. Renewable Energy 2006, 31, 249-256.
3. Satrio, D.; Utama, I.K.A.P.; Mukhtasor. Vertical axis tidal current turbine: Advantages and challenges review. 2016. [Complete journal, volume, pages, and DOI.]
4. Nicholls-Lee, R.F.; Turnock, S.R.; Boyd, S.W. Simulation-based optimisation of marine current turbine blades. 2006.
5. Ohya, Y.; Karasudani, T.; Sakurai, A.; Abe, K.; Inoue, M. Development of a shrouded wind turbine with a flanged diffuser. Journal of Wind Engineering and Industrial Aerodynamics 2008, 96, 524-539.
6. Abe, K.; Nishida, M.; Sakurai, A.; Ohya, Y.; Kihara, H.; Wada, E.; Sato, K. Experimental and numerical investigations of flow fields behind a small wind turbine with a flanged diffuser. Journal of Wind Engineering and Industrial Aerodynamics 2005, 93, 951-970.
7. Matsushima, T.; Takagi, S.; Muroyama, S. Characteristics of a highly efficient propeller type small wind turbine with a diffuser. Renewable Energy 2006, 31, 1343-1354.
8. El-Zahaby, A.M.; Kabeel, A.E.; Elsayed, S.S.; Obiaa, M.F. CFD analysis of flow fields for shrouded wind turbine diffuser models with different flange angles. Alexandria Engineering Journal 2017, 56, 171-179.
9. Al-Quraishi, B.A.J.; Asmuin, N.Z.; Mohd, S.; et al. Review on diffuser augmented wind turbine (DAWT). 2018.
10. Rahman, N.; Badshah, S.; Rafai, A.; Badshah, M. Literature review of ocean current turbine. 2014.
11. Verma, D.R.; Katkade, S.D. Horizontal axis water turbine: Generation and optimization of green energy. 2016.
12. Ghenai, C.; Salameh, T.; Janajreh, I. Modeling and simulation of shrouded horizontal-axis wind turbine using RANS method. 2017, 11(4).
13. . Cui, B.; Song, Z.; Zhang, Y.; Jin, Y.; Lin, Y. Influence of additional device on performance of the marine current turbine. 2012.
14. Gu, Y., Zou, T., Liu, H., Lin, Y., Ren, H., Li, Q., 2024. Status and challenges of marine current turbines: A global review. Journal of Marine Science and Engineering 12, 884. https://doi.org/10.3390/jmse12060884.
15. Zang, W., Zheng, Y., Zhang, Y., Lin, X., Li, Y., Fernandez-Rodriguez, E., 2023. Numerical investigation on a diffuser-augmented horizontal axis tidal stream turbine with the entropy production theory. Mathematics 11, 116. https://doi.org/10.3390/math11010116.
16. Tahani, M., Ziabakhsh Ganji, M., Simaee, M., 2023. Design and analysis of a diffuser augment horizontal axis tidal turbine for green power production. Sustainable Energy Studies. https://doi.org/10.22059/ses.2023.351567.1018.
17. Ambarita, E.E., Harinaldi, Azhari, R., Irwansyah, R., 2022. Experimental study on the optimum design of diffuser-augmented horizontal-axis tidal turbine. Clean Energy 6, 776-786. https://doi.org/10.1093/ce/zkac039.
18. Shives, M., Crawford, C., 2012. Developing an empirical model for ducted tidal turbine performance using numerical simulation results. Proceedings of the Institution of Mechanical Engineers, Part A: Journal of Power and Energy. https://doi.org/10.1177/0957650911417958.
19. Ambarita, E.E., Harinaldi, Budiarso, et al., 2021. Computational study on multi-objective optimization of the diffuser angle of a diffuser-augmented tidal turbine. Journal of Marine Science and Technology. https://doi.org/10.1007/s00773-021-00812-2.
20. Diaz-Dorado, E., Carrillo, C., Cidras, J., Roman, D., Grande, J., 2021. Performance evaluation and modelling of the Atir marine current turbine. IET Renewable Power Generation. https://doi.org/10.1049/rpg2.12071.
21. Hazim, S., Salih, A., Janan, M.T., El Ouatouati, A., Ghennioui, A., 2021. Marine current energy assessment and the hydrodynamic design of the hydrokinetic turbine for the Moroccan Mediterranean Coast. Energy Exploration & Exploitation 39, 717-737. https://doi.org/10.1177/0144598720986629.
22. Munna, S.M.F.H., Uddin, M.M., 2025. CFD analysis on horizontal axis tidal current turbine. Research on Engineering Structures and Materials 11, 3327-3339. https://doi.org/10.17515/resm2025-866en0503rs.
23. Geng, F., Zhang, X., Wang, Y., Dang, Y., He, Z., Xu, G., Che, D., Zhang, S., Wu, B., Zhu, W., 2026. A novel self-adaptive marine current turbine with a magnetically driven speed-increasing seal. Journal of Marine Science and Engineering 14, 585. https://doi.org/10.3390/jmse14060585.

24. Molland, A.F., Bahaj, A.S., Chaplin, J.R., Batten, W.M.J., 2004. Measurements and predictions of forces, pressures and cavitation on 2-D sections suitable for marine current turbines. Proceedings of the Institution of Mechanical Engineers, Part M: Journal of Engineering for the Maritime Environment 218, 127-138. https://doi.org/10.1243/1475090041651412.
25. Malki, R., Williams, A.J., Croft, T.N., Togneri, M., Masters, I., 2013. A coupled blade element momentum-computational fluid dynamics model for evaluating tidal stream turbine performance. Applied Mathematical Modelling 37, 3006-3020.
26. Myers, L., Bahaj, A.S., 2010. Experimental analysis of the flow field around horizontal axis tidal turbines by use of scale mesh disk rotor simulators. Ocean Engineering 37, 218-227.
27. Bahaj, A.S., Batten, W.M.J., McCann, G., 2007. Experimental verifications of numerical predictions for the hydrodynamic performance of horizontal axis marine current turbines. Renewable Energy 32, 2479-2490.
28. Funke, S.W., Farrell, P.E., Piggott, M.D., 2014. Tidal turbine array optimisation using the adjoint approach. Renewable Energy 63, 658-673.
29. Nishino, T., Willden, R.H.J., 2012. The efficiency of an array of tidal turbines partially blocking a wide channel. Journal of Fluid Mechanics 708, 596-606.
30. Cresswell, N.W., 2015. The generation potential of diffuser augmented tidal stream turbines. Doctoral thesis, Durham University, Durham, UK.